Observation of selective surface element substitution in $FeTe_{0.5}Se_{0.5}$ superconductor thin film exposed to ambient air by synchrotron radiation spectroscopy*

Nian Zhang(张念)[1,2], Chen Liu(刘晨)[1], Jia-Li Zhao(赵佳丽)[1], Tao Lei(雷涛)[1], Jia-Ou Wang(王嘉鸥)[1], Hai-Jie Qian(钱海杰)[1], Rui Wu(吴蕊)[1], Lei Yan(颜雷)[3], Hai-Zhong Guo(郭海中)[3], and Kurash Ibrahim(奎热西)[1,†]

[1] *Institute of High Energy of Physics, Chinese Academy of Sciences, Beijing* 100049, *China*
[2] *Shanghai Institute of Microsystem and Information Technology, Chinese Academy of Sciences, Shanghai* 200050, *China*
[3] *Institute of Physics, Chinese Academy of Sciences, Beijing* 100091, *China*

(Received 20 February 2016; revised manuscript received 10 May 2016; published online 3 August 2016)

A systematic investigation of oxidation on a superconductive $FeTe_{0.5}Se_{0.5}$ thin film, which was grown on Nb-doped $SrTiO_3$ (001) by pulsed laser deposition, has been carried out. The sample was exposed to ambient air for one month for oxidation. Macroscopically, the exposed specimen lost its superconductivity due to oxidation. The specimen was subjected to *in situ* synchrotron radiation photoelectron spectroscopy (PES) and x-ray absorption spectroscopy (XAS) measurements following cycles of annealing and argon ion etching treatments to unravel what happened in the electronic structure and composition after exposure to air. By the spectroscopic measurements, we found that the as-grown $FeTe_{0.5}Se_{0.5}$ superconductive thin film experienced an element selective substitution reaction. The oxidation preferentially proceeds through pumping out the Te and forming Fe–O bonds by O substitution of Te. In addition, our results certify that *in situ* vacuum annealing and low-energy argon ion etching methods combined with spectroscopy are suitable for depth element and valence analysis of layered structure superconductor materials.

Keywords: 11 iron-based superconductor, oxidation mechanism in ambient air, selective surface element substitution, synchrotron radiation spectroscopy

PACS: 74.25.Jb, 74.25.−q, 81.15.Fg **DOI:** 10.1088/1674-1056/25/9/097402

1. Introduction

Superconductivity in iron-chalcogenides has attracted a great deal of interest due to the high transition temperatures and the existence of antiferromagnetic order in the compounds.[1–6] Among them, the PbOtype tetragonal FeSe is regarded as an ideal material for investigating the underlying mechanism of superconductivity owing to the simple planar crystal structure and strong T_c dependence on external conditions.[7,8] For bulk material, Te substitution in the Se sites of FeSe enhances T_c up to 14 K at an optimized doping of 50% Te in the material.[9] The enhancement of T_c is attributed to the combined effects of lattice disorder arising from the substitution of large ions and electron interaction.[10,11] The T_c is shifted up to 21 K in the Fe(TeSe) thin film, which is attributed to the stoichiometry and compressive strain enhancement in the vlattice.[12,13] A further increase of the Te content diminishes the T_c and the end member FeTe is not a superconductor, instead it is an antiferromagnetic material exhibiting a spin-density wave state.[14]

Oxygen incorporation can modulate the local electronic states and superconductivity of these materials. Recently, a route to transform FeTe into a superconductor was found by directly incorporating oxygen or exposing it to air.[15–17] The experiment showed that oxygen is the only responsible agent leading to superconductivity when exposed to ambient air.[14] Only the surface region becomes superconducting, which suggests that the oxygen incorporation has a limited depth of penetration.[18] By oxidation procedures of FeTe and FeSe, it has been shown that the former gains superconductivity and the latter loses it.[17] A new observation is in contrast with the earlier work that T_c decreases even by a small amount of oxygen incorporation.[19] The less toxic nature and relatively easy synthesis compared to ironpnictides are advantageous for the applications of the (11)-type iron chalcogenide superconductors. Studying the oxidation mechanism in ambient air condition is critical for the possible applications. However, due to the difficulty in distinguishing surface contaminant and true oxidation, most works have been done with an *in situ* O_2-annealing method in a high vacuum. The oxidation layer is too thin for EDX and XRD measurements to find the changes of the chemical constituents and structures. To the best of our knowledge, the oxidation mechanism of the Fe(TeSe) superconductive thin film by exposing it to ambient air has rarely been studied.

In this paper, we report a study on the $FeTe_{0.5}Se_{0.5}$ thin film grown by the PLD method on an Nb-doped $SrTiO_3$ (001)

*Project supported by the Chinese Academy of Sciences (Grant No. 1G2009312311750101) and the National Natural Science Foundation of China (Grant Nos. 11375228, 11204303, and U1332105).

†Corresponding author. E-mail: kurash@ihep.ac.cn

© 2016 Chinese Physical Society and IOP Publishing Ltd

substrate, which was exposed to ambient air for one month. We focus on the influence of the oxygen incorporation in the film. We observe an element selective substitution reaction on the surface of the thin film. By a series of *in situ* methods, such as argon ion etching, vacuum annealing, photoelectron emission spectroscopy (PES) measurement and x-ray absorption spectroscopy (XAS), we investigate the characteristic modifications that occurred in the electronic structure.

2. Experiment

The thin film preparation and *in situ* electronic structural characterization associated with complementary methods after the *ex situ* exposure to air have been carried out in a recently commissioned comprehensive PES endstation system on beamline 4B9B of the Beijing Synchrotron Radiation Facility (BSRF). The actual experimental process is schematically depicted in Fig. 1. The 100 nm $FeTe_{0.5}Se_{0.5}$ thin film was grown on an Nb-doped $SrTiO_3$ (001) substrate by PLD using a nominal 1:0.55:0.55 Fe–Te–Se composition target.[20] The substrate was ultrasonically cleaned in acetone and ethanol before being put into the chamber with a base pressure of 6×10^{-10} torr. The STO was degassed at 500 °C for 1 h[21] and cooled down to 350 °C for $FeTe_{0.5}Se_{0.5}$ growth. The laser (355 nm wavelength) was operated at the repetition rate of 4 Hz and laser energy of 80 mJ/pulse. The target–substrate distance was 6 cm. The stoichiometry of the grown film was about $FeTe_{0.42}Se_{0.65}$ very close to $FeTe_{0.5}Se_{0.5}$ as detected by EDX. The film was immediately transferred from the PLD growth chamber to the analysis chamber for *in-situ* PES and XAS measurements. All the PES measurements were performed with 900 eV photon energy and the XAS were measured in the total electron yield (TEY) mode.

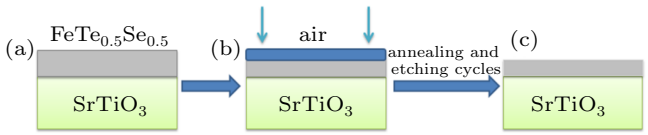


Fig. 1. (color online) A schematic representation of experimental processes. (a) A 100 nm superconductive thin film was deposited by the PLD method on an Nb-doped STO substrate. (b) The film was exposed to ambient air at room temperature in a super-clean laboratory for one month. (c) The air-contacted film was re-introduced into the ultrahigh vacuum chamber and was subjected to cycles of annealing and etching treatments, which was followed by subsequential electronic structure measurements.

Following exposure to ambient air at room temperature in a super-clean laboratory for one month, the thin film was again introduced into the ultrahigh vacuum chamber to inspect the effects of air in terms of the microscopic characters of the film. To remove the contamination and oxidation layers, the film was treated by a vacuum annealing and argon ion etching procedure. The procedure contains three steps: 1) 1st annealing at the deposition temperature 350 °C for 30 min, 2) argon ion etching for 30 min, 3) 2nd annealing at the deposition temperature 350 °C for 30 min. The argon ion was accelerated at 1000 V field with the working pressure kept at 3×10^{-6} mbar.

3. Results and discussion

The electric resistance measurement results of the as-grown, exposed-to-air, and after-treatment films at various temperatures are shown in Fig. 2. The as-grown film shows a superconducting transition with $T_c^{onset} = 15.8$ K, its resistivity variation with temperature shows a weakly metallic behavior consistent with that of bulk $FeTe_{0.5}Se_{0.5}$.[22] The superconductivity disappears in the exposed-to-air thin film, it shows a continuous increase of resistivity with the temperature lowering. The resistivity of the after-treatment film shows a steady increase similar to that of the exposed-to-air film, while the resistivity increasing ratio is apparently high, which may be caused by the decrease of the thickness (about 55 nm after the treatments).[12] The change of the elementary composition in the deep layer and the broken crystal structure on the surface after the treatments may also influence the film's resistivity, leading to the un-recovery superconductivity. Microscopic origins of such a change are investigated from the point view of the electronic structure in the following sections.

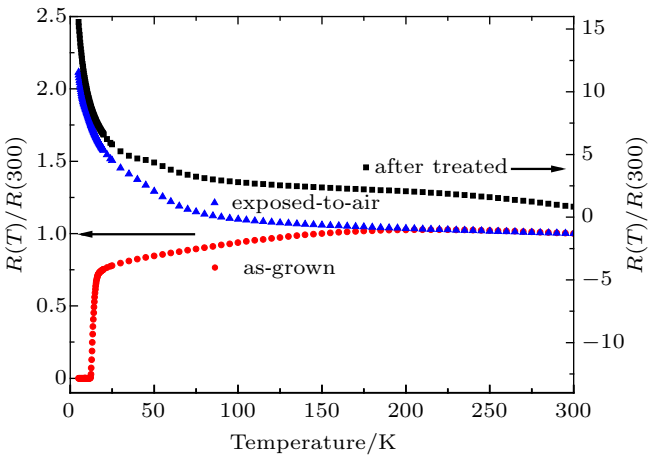


Fig. 2. (color online) Electric resistance versus temperature of the as-grown, exposed-to-air, and after-treatment films. The as-grown, exposed-to-air, and after-treatment films are respectively obtained after steps (a)–(c) in Fig. 1.

The whole elemental wide scan PES results of the film at different stages are given in Fig. 3. The spectrum of the as-grown film shows only the three native Fe, Te, and Se elements, while the exposed-to-air sample shows nothing pertaining to the thin film except O and C introduced as a result of contaminations. The result after the 1st annealed step can be used to distinguish physisorption and chemisorption contaminations. The disappearance of the C contaminant and the increase of the O portion reflect that the C and O really exist in distinguished binding environments. The easy desorption

of the C contaminant by vacuum annealing at 350 °C indicates that it is purely in the physisorption state, whereas the O is in the chemisorption state.

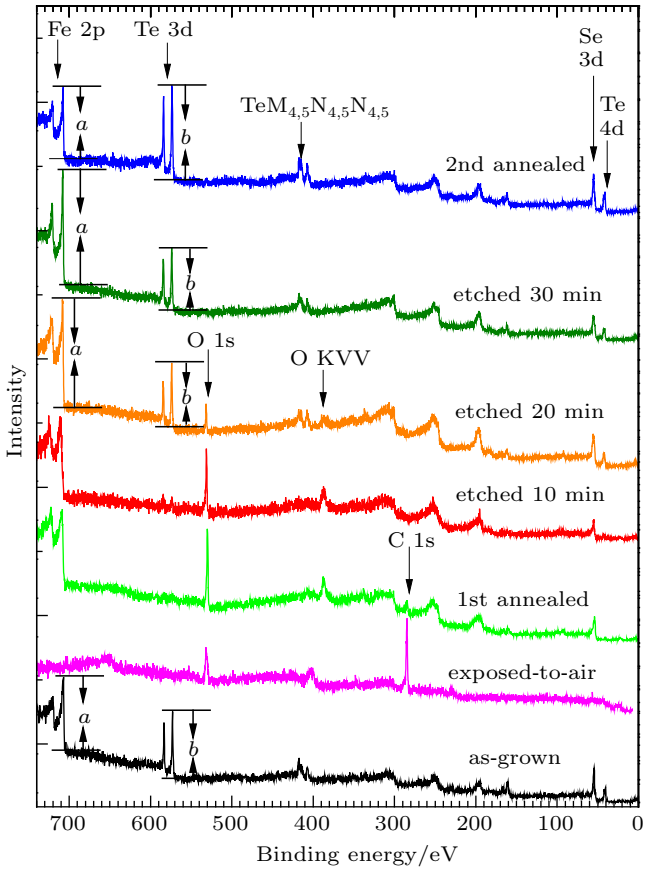


Fig. 3. (color online) Wide scan all element including PES results of the thin film shown from bottom to top in the order of the film being treated: as-grown, exposed to air, first time annealed at 350 °C for 30 min, etched for 10 min, etched for 20 min, etched for 30 min, and vacuum annealed again at 350 °C for 30 min before being taken out of the ultrahigh vacuum chamber for the after-treated T_c measurements.

Surprisingly, two of the three native elements of the as-grown film Fe and Se re-emerge along with the O, missing the signal of Te in the annealed and etched for 10 min spectra. A lack of Te and the existence of O in place of Te in the form of chemisorption indicate that Te in the film is substituted by O, and the substitution degree changes from complete in the top layers to partial in the deeper layers of the film. This point can be visualized by the spectra after the argon ion etching. With the 10 min etching, the O intensity decreases apparently but the Te stays hidden in the measurement region, implying that the layers removed by this process contain only FeSe/O. When the aggregated etching time reaches 20 min, the oxygen diminishes and at the same time the Te begins to appear, the layers show the multi-elemental FeTeSe/O situation. With another 10 min etching, the exotic oxygen element disappears thoroughly.

From the spectra measured following the sequential dynamic treatment processes, another prominent evidence shows up that the element compositional ratios in the measured depth region change with the treatment process. As can be seen in Fig. 4, the relative elemental ratios to reflect changes of Fe/Te by intensity of a/b in Fig. 3 fluctuate between large and small values, it is 1.083 in the as-grown surface, 1.675 in the Te and O coexisting phase, 1.808 in the surface etched for 30 min, and 0.767 after annealing for 30 min. During the etching process, the intensity of the Te peak increases while the ratio Te/Fe decreases. The reason is that Te rarely exists in the surface layers because of the substitution of O and increases with the etching depth, but the etching process preferentially removes ligand elements around the central Fe ion and results in Fe enriching and anions defect states on the surface at the same time, which lead to a larger increase of Fe intensity than that of Te. To confirm the influence caused by etching and vacuum annealing, we performed the same treatments on the as-grown film for comparison (red points in Fig. 4). When etched at 1000 V for 10 min, Fe/Te increases to 2.032 and does not obviously change with the etching time. It is not surprising that in the etching treatment processes, the ionized argon ions impinging on the surface with 1000 eV potential energy have heterogeneous effects on the multi-element composition surface. The most direct consequence for the etching procedure is that an effective collision with larger probability happens between Ar^+ and anion ligand elements (Se^{2-}, Te^{2-}, and O^{2-}) instead of with Fe^{2+} due to the repelling effect between the plus charge atoms; the etching ratio for Fe and Te is stable in this material. Secondly, the weaker the binding energy of the anion to the cation in the crystal lattice, the easier the binding bond to be broken by the collision. Thirdly, the smaller the mass of the anion among the constituent elements, the easier it is knocked out from the crystal lattice. All three points get a meaningful footnote in the spectra etched for 20 min and 30 min with the Fe/Te relative ratios in the oxidized sample change from 1.675 to 1.808.

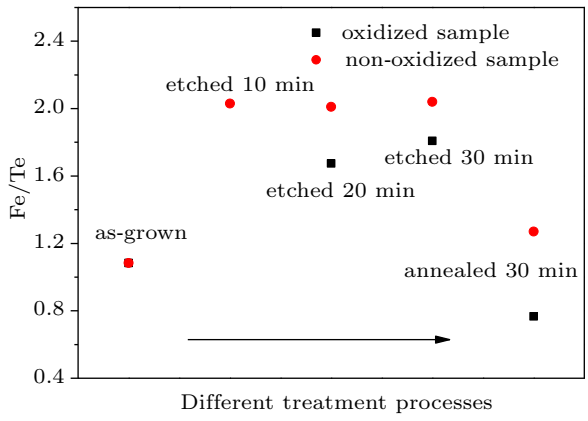


Fig. 4. (color online) The variation of Fe/Te ratio caused by different treatments for the oxidized sample (black points) and the non-oxidized sample (red points) detected by XPS.

A straight consequential result in the thermodynamic effect on the after-treated phase in the oxidized sample shows

up in the 2nd annealing by the Fe/Te ratio dropping to 0.767. The variation tendency is similar to that of the non-oxidized sample in which Fe/Te significantly decreases from 2.041 to 1.234 after vacuum annealing. We have confirmed that annealing at the deposition temperature (350 °C) does not affect the as-grown film, the 2nd annealing thus plays the role of mobilizing chalcogenide elements to segregate from chalcogenide rich deep layers under the defect rich surface to fill the defect sides, and then converge at the surface of the thin film, which creates an Fe defect surface area.

We encountered the oxidation-reduction evolution of the as-grown film from being exposed to air through sequential steps of treatment, what is not yet clearly elucidated evolution behavior accompanying these processes is the valence state variation of the central atom Fe. To achieve this goal, we inspect the variation by electronic structure investigation through fine scanned Fe 2p PES and Fe $L_{2,3}$ XAS measurements.

Determining the valence state or tracking the valence state variation of the Fe within different chemical environments through PES and XAS spectra is a complex and nontrivial issue.[23–27] The same Fe 2p core level in the same stoichiometric chemical form can have largely different binding energies owing to various follow-up extrinsic or intrinsic conditions related to the measurement results, for example, the crystal form of the substance such as film, powder, or single crystal; the preparation condition of the specimen such as *in situ* or *ex situ*; the character of the bond types such as ionic, strong, or weak covalent depending on the electronegativity of the anion elements; the sophisticated higher order interactions between Fe and anions apart from incipient chemical reactions such as crystal field, Mott–Hubbard or charge transfer. No comparable experimental results measured under the resemble conditions as depicted in Fig. 1 are available for the $FeTe_{0.5}Se_{0.5}$ system in the literature, neither are reference binding energies in tabulated values.[28] We are going to take the results of iron oxides by PES[23,24] and XAS,[25–27] where the iron oxide systems have been investigated systematically in a comparable way to the underlying system, as an analogous reference to single out information on the Fe valence state variation in the actual processes.

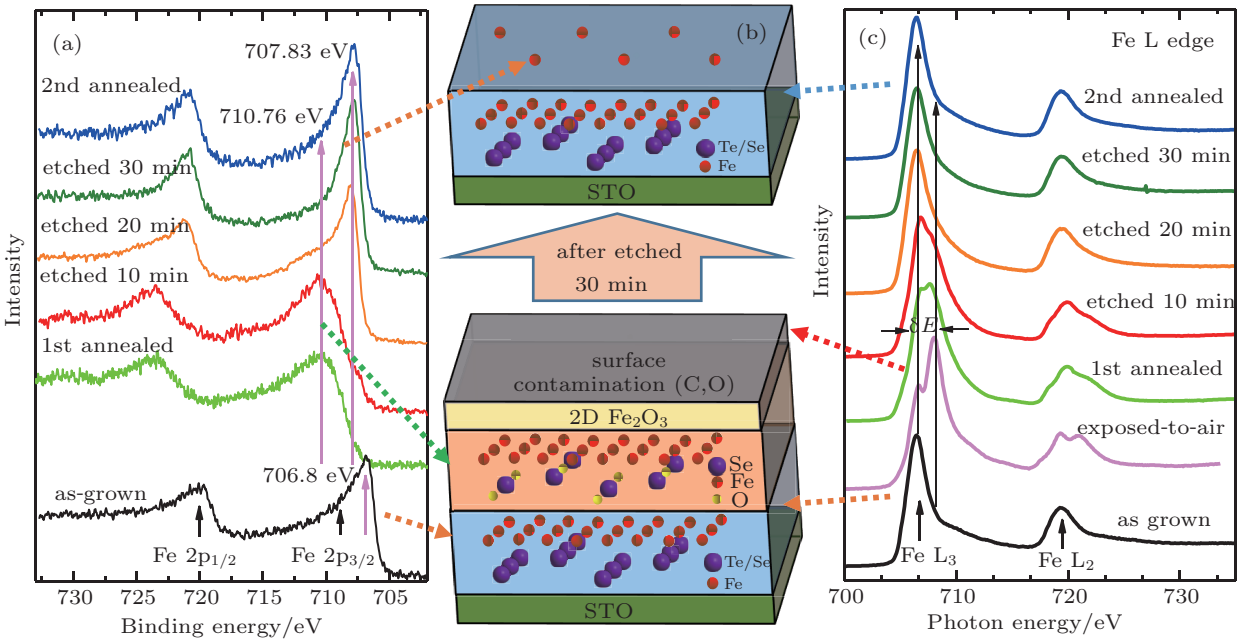


Fig. 5. (color online) (a) Fe-2p PES spectra measured in the order of the specimen treatment process from bottom to top. (b) Schematic of the oxidized thin film and the variation caused by vacuum treatments revealed by PES and XAS results. A quasi-2D Fe_2O_3 layer forms on the fully oxidized surface and a layer that Te is totally substituted by O beneath it. After being etched for 30 min, the O is totally removed from the film, leaving excess iron on the surface caused by the etching process. (c) Fe $L_{2,3}$ ($2p_{3/2}$ and $2p_{1/2}$ levels) XAS spectra measured in the order of specimen treatment processes from bottom to top. $\delta E = 708.1 - 706.46 = 1.55$ eV.

In the PES spectra of Fe 2p shown in Fig. 5(a), we observe that the $2p_{3/2}$ region has three distinctly separated peaks at binding energies 706.8 eV, 707.83 eV, and 710.76 eV as labelled with arrows. The evolution of these three peaks' intensities with the treatment steps unravels the variation of both the stoichiometric composition and the valence state of iron along with the processes. At the 1st annealed stage, where the on surface physically absorbed contaminants are cleared up as shown in Fig. 3, the intense 710.76 eV binding energy peak demonstrates strong evidence for the existence of Fe^{3+} states in the surface, which cannot be reduced through vacuum annealing. When the 1st annealed surface is etched for 10 min, in

addition to the main peak in the spectrum, one observes a weak shoulder at 707.83 eV, which is characteristic of Fe^{2+}. The unchanged main peak position represents an important fact that vacuum annealing and argon ion etching are similar and which do not induce a reduction reaction to the thin film. The result confirms that it is reliable to use vacuum annealing and argon ion etching for depth valence analysis of layer structure superconductor thin film. The weak shoulder peak at 707.83 eV in this step then eventually becomes the main one accompanying with the appearance of Te following the aggregation of the surface etching time from 10 min through 30 min, we speculate that the substitution effect probably happens after the Fe is totally oxidized to the +3 state. However, the peak position does not recover to 706.8 eV as in the as-grown $FeTe_{0.5}Se_{0.5}$ even the oxygen is totally removed which may be one of the reasons for the disappearance of superconductivity.

Due to the apparent difference in the detection length for XAS ($\sim$ 10 nm) and PES ($\sim$ 2–3 nm) measurements, we observe a more complicated spectral structure in the XAS spectra shown in Fig. 5(c). The XAS spectrum of the exposed-to-air sample has characteristics of Fe^{3+}-valence state similar to Fe_2O_3 by the Fe $2p_{3/2}$ (i.e. the L_3) edge showing $t_{2g}\downarrow$ and $e_g\downarrow$ two-peak structure.[26,27] However, the energy separation between the $t_{2g}\downarrow$ and $e_g\downarrow$ states, which is called the octahedral crystal field 10Dq value, is 1.55 eV for the exposed film, not equivalent to the Fe_2O_3 bulk system 1.45 eV.[26,27] In our PES spectra, the iron stays at the Fe^{3+} state during the 1st annealing procedure and we do not observe significant changes until etching for 20 min, but the XAS spectra show variations just after the 1st annealing, which indicates that Fe^{3+} stays at least in two different chemical environments. This might be understood in terms of the very thin (less than the investigation depth of XAS) fully oxidized layer of quasi-2D Fe_2O_3, the crystal field in which the Fe–ligand interactions is modulated by the crystal field of Fe^{3+}–Se–O underneath, leading to $\delta E = 1.55$ eV.

Te is reported to evolve from a purely metallic state to a mixed Te/Te^{4+} state as a function of air exposure or oxygen annealing.[17,29] We could hardly detect the signal of Te in the very surface of the exposed thin film without treatment. In Fig. 6, the Te $3d_{5/2}$ peaks in the as-grown film and during treatments are all maximum at a binding energy of 572.9 eV, Te $3d_{3/2}$ peak at 583.45 eV and Se 3d peak at 54.6 eV, in excellent agreement with the literature for metallic Te and Se,[17] indicating that all the elements stay at the metallic state. A clear enhancement of the shoulder arrowed in Fig. 6(b) at 52.9 eV through the etching procedure is observed which is due to the influence of the zero state Fe 3p peak.[29,30] The observation supports effective collision with larger probability between Ar^+ and anion ligand elements (Se^{2-}, Te^{2-}, and O^{2-}), instead of with Fe^{2+} due to the repelling effect between the plus charge atoms. The excess iron is left on the surface of the etched film, which leads to the appearance of the peak at 52.9 eV. Our results suggest that the peak position 706.8 eV of the Fe $2p_{3/2}$ electron, which is quite similar to metallic iron, seems to be crucial to the superconductor property instead of nominal Fe^{2+}. Electrons of iron in $FeTe_{0.5}Se_{0.5}$ thin film more likely stay in a metal crystal that delocalize and roam around the crystalline lattices but not totally equal to metallic ones as the difference can be observed in the Fe 3p peak.

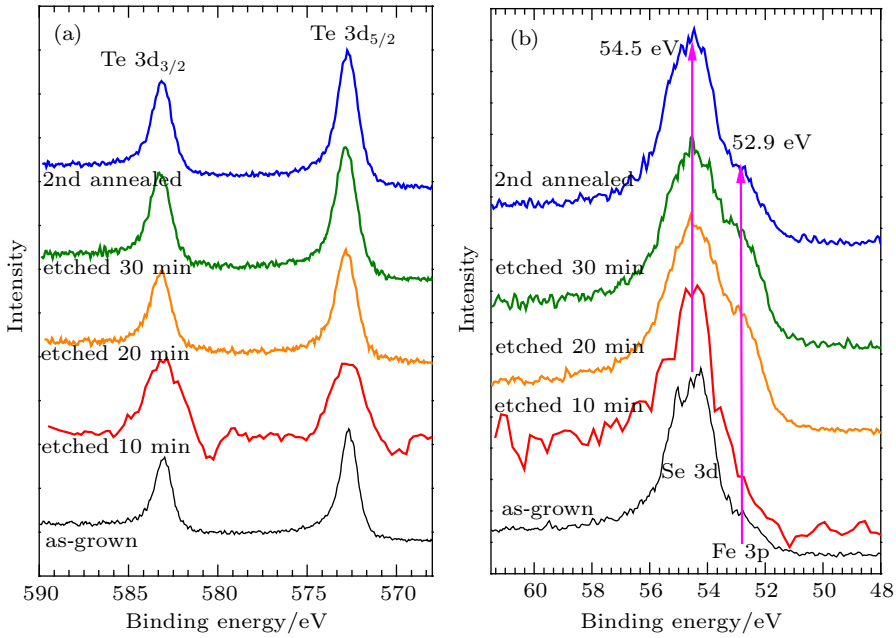


Fig. 6. (color online) (a) The variation of Te-3d spectra with the increase of the etching thickness and after vacuum annealing. (b) Se-3d and Fe-3p spectra with the increase of the etching thickness and after vacuum annealing compared with those of the as-grown film, a peak at 52.9 eV appears after etching and decreases after annealing.

A series of data through surface treating processes show that the vacuum annealing and argon ion etching have created an imbalanced element distribution, but do not induce the impact of the valence state to the material, which make the methods suitable for depth valence analysis for these materials. However, we tried the treatments on non-oxidized and oxidized samples, superconductivity cannot be retained in both samples. The etching treatments damage the crystal structure on the surface, the last step of annealing is not able to restore the as-grown crystal phase as the peak position of Fe is unable to go back to 706.8 eV, instead it redistributes the chalcogenide defects created by the etching process in a larger scale in the crystal lattice. Te in the deep layers may diffuse to the surface to fill the defects through annealing, which may account for the unrecovered superconductivity. Moreover, the decrease of the film thickness after etching and the enriched iron in the deep layer after Te diffusion may also be the reasons for the disappearance of superconductivity and the rapid increase of resistance at low temperature.

4. Conclusion

We investigated the excess oxidation mechanism of $FeTe_{0.5}Se_{0.5}$ superconductor thin film exposing in ambient air. Oxygen selectively breaks the chemical bonds between Fe and Te after excessive oxidation, which oxidizes Fe to the +3 state and makes Te unstable in the surface. Se is not obviously influenced, which means different responses of the respective chalcogenides to oxidation in $FeTe_{0.5}Se_{0.5}$ and the Fe–Se band is much stronger than Fe–Te in this system. The disappearance of superconductivity is related to the substitution of tellurium by oxygen, which forms 2D Fe_2O_3 and FeSe:O layers in the surface of the thin film. The spectroscopic data herein emphasizes the significance of itinerant electrons in iron to the superconductivity property. Vacuum annealing and argon ion etching as common treatments do not induce impact of the valence state to the oxidized $FeTe_{0.5}Se_{0.5}$ thin film, which confirms their reliability in the depth element and valence analysis of layer-structure superconductor materials.

References

[1] Kamihara Y, Watanabe T, Hirano M and Hosono H 2008 *J. Am. Chem. Soc.* **130** 3296

[2] Subedi A, Zhang L, Singh D J and Du M H 2008 *Phys. Rev. B* **78** 134514

[3] Wei Z, Li H o, Hong W, Lv Z, Wu H, Guo X and Ruan K 2008 *J. Supercond. Novel Magn.* **21** 213

[4] Fang M H, Pham H M, Qian B, Liu T J, Vehstedt E K, Liu Y, Spinu L and Mao Z Q 2008 *Phys. Rev. B* **78** 224503

[5] Bao W 2013 *Chin. Phys. B* **22** 087405

[6] Liu Z H, Cai Y P, Zhao Y G, Jia L L and Wang S C 2013 *Chin. Phys. B* **22** 087406

[7] Imai T, Ahilan K, Ning F, McQueen T and Cava R 2009 *Phys. Rev. Lett.* **102** 177005

[8] Medvedev S, McQueen T, Troyan I, Palasyuk T, Eremets M, Cava R, Naghavi S, Casper F, Ksenofontov V and Wortmann G 2009 *Nat. Mater.* **8** 630

[9] Ding Q P, Mohan S, Tsuchiya Y, Taen T, Nakajima Y and Tamegai T 2011 *Supercond. Sci. Technol.* **24** 075025

[10] Chen C L, Dong C L, Chen J L, Guo J H, Yang W L, Hsu C C, Yeh K W, Huang T W, Mok B H, Chan T S, Lee J F, Chang C L, Rao S M and Wu M K 2011 *Phys. Chem. Chem. Phys.* **13** 15666

[11] Mizuguchi Y, Hara Y, Deguchi K, Tsuda S, Yamaguchi T, Takeda K, Kotegawa H, Tou H and Takano Y 2010 *Supercond. Sci. Technol.* **23** 054013

[12] Bellingeri E, Pallecchi I, Buzio R, Gerbi A, Marrè D, Cimberle M R, Tropeano M, Putti M, Palenzona A and Ferdeghini C 2010 *Appl. Phys. Lett.* **96** 102512

[13] Zhuang J, Yeoh W K, Cui X, Xu X, Du Y, Shi Z, Ringer S P, Wang X and Dou S X 2014 *Sci. Rep.* **4** 7273

[14] Nie Y F, Telesca D, Budnick J I, Sinkovic B and Wells B O 2010 *Phys. Rev. B* **82** 020508(R)

[15] Si W, Jie Q, Wu L, Zhou J, Gu G, Johnson P D and Li Q 2010 *Phys. Rev. B* **81** 092506

[16] Narangammana L K, Liu X, Nie Y F, Rueckert F J, Budnick J I, Hines W A, Gu G and Wells B O 2013 *Appl. Phys. Lett.* **103** 102604

[17] Telesca D, Nie Y, Budnick J I, Wells B O and Sinkovic B 2012 *Phys. Rev. B* **85** 214517

[18] Sun Y, Tsuchiya Y, Taen T, Yamada T, Pyon S, Sugimoto A, Ekino T, Shi Z and Tamegai T 2014 *Sci. Rep.* **4** 4585

[19] Thakur G S, Haque Z, Neha P, Gupta L C, Patnaik S and Ganguli A K 2014 *Z. Anorg. Allg. Chem.* **640** 1159

[20] Zhang N, Wang J O, Lei T, Liu C, Zhang S H, Qian H J, Wu R, Zhou H, Wang H Q, Zheng J C, Guo H Z, Yan L and Ibrahim K 2015 *AIP Advances* **5** 047149

[21] Zhang S H, Wang J O, Qian H J, Wu R, Zhang N, Lei T, Liu C and Kurash I 2015 *Chin. Phys. B* **24** 027901

[22] Yeh K W, Huang T W, Huang Y l, Chen T K, Hsu F C, Wu P M, Lee Y C, Chu Y Y, Chen C L, Luo J Y, Yan D C and Wu a M K 2008 *Europhys. Lett.* **84** 37002

[23] Descostes M, Mercier F, Thromat N, Beaucaire C and Gautier-Soyer M 2000 *Appl. Surf. Sci.* **165** 288

[24] Yamashita T and Hayes P 2008 *Appl. Surf. Sci.* **254** 2441

[25] de Groot F M F, Fuggle J C, Thole B T and Sawatzky G A 1990 *Phys. Rev. B* **42** 5459

[26] Miedema P S and de Groot F M F 2013 *J. Electron. Spectrosc. Relat. Phenom.* **187** 32

[27] Zhu X, Kalirai S S, Hitchcock A P and Bazylinski D A 2015 *J. Electron. Spectrosc. Relat. Phenom.* **199** 19

[28] http://srdata.nist.gov/xps/main_search_menu.aspx

[29] Su T S, Yin Y W, Teng M L, Gong Z Z, Zhang M J and Li X G 2013 *J. Appl. Phys.* **114** 183901

[30] Lad R and Henrich V 1989 *Phys. Rev. B* **39** 13478